JMEPEG (2023) 32:2598–2606
https://doi.org/10.1007/s11665-022-06853-x

1059-9495/$19.00

TECHNICAL ARTICLE

Effect of Nd on the Microstructure and Mechanical Properties of Mg-La-Ce Alloys at Ambient and Elevated Temperatures

Lingyun Feng, Xixi Dong, Qing Cai, Bin Wang, and Shouxun Ji

Submitted: 24 January 2022 / Revised: 27 February 2022 / Accepted: 11 March 2022 / Published online: 8 April 2022

The microstructures and tensile properties were investigated for high-pressure die-cast Mg1.6La1.0Ce alloy with different Nd contents from 0 to 3 wt.%. The results showed that fine dendritic and segmented dendritic microstructures were observed in the as-cast alloys, but the eutectic morphology changed from lamellar for low Nd-containing alloys to continuous fibrous with dendritic α-Mg in eutectics for high Nd-containing alloys. The compositions of the eutectic phase were also transferred from Mg_{12}(La, Ce) in the alloys without Nd to Mg_{12}(La, Ce, Nd) in the alloys with Nd addition. When the concentration of Nd was greater than 2 wt.%, numerous nanoscale Mg-Nd intermetallic phases precipitated at the grain boundaries and eutectic area. The addition of Nd was also found to increase tensile strength significantly at ambient temperature and elevated temperatures. For the alloy without Nd, the yield strength and ultimate tensile strength (UTS) was 135.6 MPa and 189.9 MPa at ambient temperature and 56.3 MPa and 57.4 MPa at 300 °C, respectively. When adding 3 wt.% Nd, the yield strength increased to 161.9 MPa at ambient temperature and 75.4 MPa at 300 °C. The UTS increased to 181.9 MPa at ambient temperature and 90.4 MPa at 300 °C. The significant improvement in strength was attributed to the strengthening from the refined structure and the dispersion of second-phases of intermetallic compounds.

Keywords elevated temperatures, magnesium alloys, mechanical properties, microstructures, strengthening mechanism

1. Introduction

Magnesium alloys have been widely accepted as promising lightweight materials and therefore have found extensive applications in industry such as transport and electronic manufacturing (Ref 1, 2, 3). However, the commercial applications of magnesium alloys are still marginally under the expectation due to the low mechanical properties at ambient and elevated temperatures (Ref 3). One of the practical approaches to improve the mechanical properties of Mg alloys is alloying, by which appropriate elements are introduced into alloys to enhance strengthening (Ref 1, 2). As such, extensive research to understand the role of alloying elements on the microstructures and resultant mechanical properties of Mg alloys at ambient and elevated temperatures have been conducted worldwide in recent years (Ref 1, 2, 3).

The existing studies for alloying Mg alloys have covered several elements, in which the main concerns were mainly focusing on rare earth elements because of the particular features in Mg alloys. The influence of rare earth elements on the microstructures, thermal conductivity, corrosion performance, tensile properties, creep features of different Mg alloys have been reported for La (Ref 4, 5, 6), Ce (Ref 7, 8), Pr (Ref 9, 10)(Ref 11), Nd (Ref 12, 13), Gd (Ref 14, 15), Er (Ref 16, 17, 18), Yb (Ref 19), Sm (Ref 20, 21), Y(Ref 22, 23, 24) and Sc (Ref 25, 26). Generally, the effect of rare earth elements in Mg alloys is different according to the solubility, and the conclusions are somehow different. The elements with low solubility in the Mg matrix offer limited solution strengthening and precipitate strengthening. The excess elements react with other alloying elements to form Re-containing particles to strengthen secondary phases, significantly affecting the microstructures and tensile properties of Mg alloys (Ref 1).

As an essential rare earth element, Nd has recently attracted considerable attention. Arrabal et al. (Ref 27) studied the corrosion performance of AZ91 alloy with Nd addition and found Nd can suppress the galvanic corrosion between a-Mg and secondary phases. Lei (Ref 13) studied the microstructure and mechanical properties of extruded Mg-4Gd-0.5Zr-*x*Nd alloy. The addition of Nd weakens the texture and decreases the intensity of texture. The substantial increase in strength without scarifying the elongation-to-failure because of the contribution of fine dispersed $Mg_{41}Nd_5$ and Mg_{12}(Nd, Gd) particles in the matrix. Wang et al. (Ref 28) found that Nd leads to the uniformity of microstructure in Mg-2Zn-0.46Y-0.5Nd alloy and can improve the tensile property and enhance the corrosion

This invited article is part of a special topical focus in the *Journal of Materials Engineering and Performance* on Magnesium. The issue was organised by Prof. C. (Ravi) Ravindran, Dr. Raja Roy, Mr. Payam Emadi and Mr. Bernoulli Andilab, Ryerson University.

Lingyun Feng, Xixi Dong, Qing Cai, and **Shouxun Ji**, Brunel Centre for Advanced Solidification Technology (BCAST), Brunel University London, Uxbridge Middlesex, London UB8 3PH, UK; and **Bin Wang**, Department of Mechanical Engineering and Aerospace, Brunel University London, Uxbridge Middlesex, London UB8 3PH, UK. Contact e-mail: Xixi.Dong@brunel.ac.uk.

resistance of Mg-2Zn-0.46Y-1.0Nd alloy. Su et al. (Ref 29) found that the thermal conductivity of as-cast Mg-Nd alloys is higher than that of T4 counterparts while lower than that of corresponding T6 alloys. Ning (Ref 30) found Nd increases the mechanical properties at elevated Mg-0.3Zn-0.32Zr alloy temperatures. The existence of the Mg_{12}(Nd, Zn) phase within the grains and along the grain boundaries for the alloys containing high Nd acts to lock the grain boundaries and reduce grain boundary and dislocation sliding at elevated temperatures. Mo et al. (Ref 31) found that Nd modified Mg-3Gd-2Ca alloy after solid solution treatment can remarkably improve the creep resistance at 210 °C. Hence, it is confirmed that Nd additions to different Mg alloys have different effects on their microstructures and tensile properties.

From these studies, most of the existing works tend to focus on one Mg alloy property that includes high rare earth elements, which inevitably increases the cost of Mg alloys. Therefore, it is necessary to consider multiple properties simultaneously for the cast Mg alloys with less rare earth elements. Therefore, the present study aims to investigate the effect of Nd on the microstructures and tensile properties at ambient and elevated temperatures for the high-pressure die-cast Mg-1.6wt.%La-1.0wt.%Ce-*x*Nd alloys from 0 to 3 wt.%. The discussion is focused on the strengthening mechanisms and relationship between the microstructure and strength in the Mg alloys.

2. Experimental

Pure Mg (99.9 wt.%), pure Zn (99.5 wt.%), Mg-30 wt.% Gd and Mg-25 wt.% Ce master alloys were used to make the Mg-1.6wt.%La-1.0wt.%Ce alloy with various Nd additions. The alloy composition was weighted with specific ratios and melted in a resistance furnace under an atmosphere containing 0.5%SF_6 in N_2 gas at 720 °C. After homogenization and skimming, a mushroom sample was made to measure the chemical composition before casting. ICP-OES determined the final compositions, and the results are shown in Table 1.

The casting was made on a 4500 KN cold chamber high-pressure die casting machine, during which the melt was manually dosed and subsequently released into the shot sleeve. During casting, the die was pre-heated by the circulation of mineral oil at 200 °C, and the intensification stress was set as 320 mpa. And the melt was fully monitored with a pouring temperature of 715 °C by a K-type thermocouple. Eight ASTM standard φ6.35-mm-round and 50–mm-gauge length samples were cast in each shot.

Table 1 Chemical composition of the experimental Mg1.6La1Ce-*x*Nd alloys obtained by ICP-OES

Alloy	*x*	La	Ce	Nd	Zn	Mn	Mg
Mg1.6La1Ce-0Nd	0	1.61	0.94	0.02	0.26	0.23	Bal.
Mg1.6La1Ce-0.5Nd	0.5	1.52	0.95	0.51	0.23	0.26	Bal.
Mg1.6La1Ce-1Nd	1	1.56	0.94	0.98	0.28	0.25	Bal.
Mg1.6La1Ce-2Nd	2	1.53	0.97	2.04	0.25	0.26	Bal.
Mg1.6La1Ce-3Nd	3	1.55	0.95	2.95	0.27	0.25	Bal.

The tensile tests were conducted following the ASTM B557-15 and ASTM E8/E8M-16 standard using an Instron 5500 Universal Electromechanical Testing Systems equipped with Bluehill software and a 50 KN load cell. All the tests were performed at ambient temperature (20 °C) and elevated temperature (250 and 300 °C). The extensometer's gauge length was 50 mm, and the ramp rate for extension was 1 mm/min at ambient temperature and 0.0002/s at elevated temperature. Each data reported is based on the properties obtained from 5 samples.

The middle part of the tensile bars was cut for microstructural examination using a Zeiss optical microscopy with quantitative metallography and a Zeiss SUPRA 35VP scanning electron microscope (SEM) equipped with Energy Dispersive x-ray (EDX). SEM analysis was performed with an accelerating voltage of 20 kV on a polished sample for morphology observation at backscattered electron (BSE) mode and the fracture surface at secondary electron (SE) mode. 3-mm-round samples were polished to 50-μm-thick and then ion thinned with the Gatan precision ion polishing system (PIPS) at a voltage of 3-5KV and an angle of 3-5°. The thinned samples were used for selected diffraction (SAED), bright field (BF), high resolution and EDX analysis with a transmission electron microscope (TEM) JEOL 2100F. ImageJ software was used to measure the volume fraction and the grain size of phases.

3. Results

3.1 Phase Analysis

Figure 1 shows the XRD spectra for the experimental as-cast Mg1.6La1Ce alloy with different Nd contents. The alloys presented two types of diffraction peaks of α-Mg and Mg_{12}RE phase. It is clear that adding the Nd element did not generate a new phase in the Mg alloys. However, the diffraction peaks of the Mg_{12}RE phase were intensified gradually with the increase of Nd addition, indicating that more Mg_{12}RE phase was generated in the as-cast alloys. Therefore, the amount of Nd in the as-cast alloys can be an approach to control alloy performance.

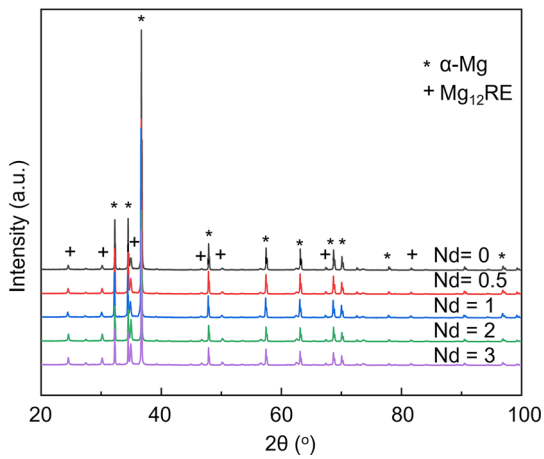

Fig. 1 XRD results of the as-cast die-cast Mg1.6La1Ce-*x*Nd alloys

3.2 Microstructure Observations

In Fig. 2(a)-(e), it is evident that the microstructure of all the alloys in this study consists of α-Mg and interdendritic eutectic phases on grain boundaries. Fine dendritic and segmented dendritic microstructures were observed in all the as-cast alloys. Two different grain sizes are evident in the alloys. The average grain size of the Mg1.6La1Ce alloy was approximately 8.8 μm, with the larger grains up to 35 μm. The grain size was further slightly refined with the addition of Nd. With 3% Nd addition, the grain size of the alloy was approximately 5.6 μm, while the larger grains were refined to approximately 20 μm. The difference in grain size in the alloys was mainly caused by the different cooling rates in HPDC (Ref 32). Figure 2(f)-(j) shows that the eutectic in the Mg1.6La1Ce-*x*Nd alloy had an interconnected structure. As the Nd content increased, the eutectic structure was not changed and remained continuous and fibrous eutectic, but there was a significant increase in the eutectic regions. The volume fraction of the intermetallic compound gradually increased with the addition of Nd, as measured by SEM-BSE images with ImageJ software in Fig. 3. The variation in volume fraction remained consistent with the behaviour in the binary Mg-Nd alloy and Mg-La-Nd alloys (Ref 33, 34).

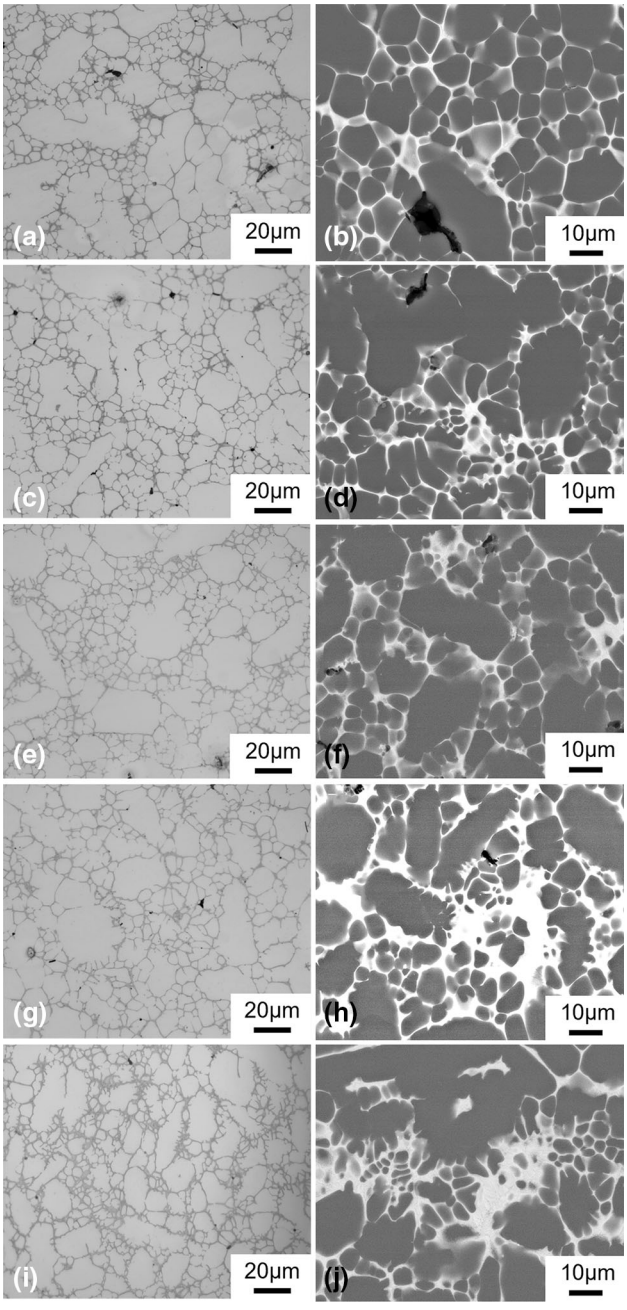

Fig. 2 Optical microstructure and BSE-SEM microstructure of the as-cast die-cast Mg1.6La1Ce-*x*Nd(x = 0, 0.5, 1, 2, 3) alloys; (a), (b) x = 0 Nd, (c), (d) x = 0.5 Nd, (e), (f) x = 1 Nd, (g), (h) x = 2 Nd, (i), (j) x = 3 Nd

Further observations of the eutectic morphology at high magnification of SEM-BSE revealed that, in the absence of Nd addition, α-Mg in eutectic showed a mixture of rod-like and lamellar structures between the intermetallic compounds in Fig. 4(a). With the addition of Nd, the α-Mg structure in eutectic was transformed into dendritic and devoiced structure. In addition, the addition of Nd resulted in the appearance of a bulk intermetallic compounds in the eutectic region with a significantly higher brightness than the previously observed eutectic phase. Figure 4(b)-(d) shows that the bulk phases can be seen relatively clearly with the 2.0 wt.% Nd addition compared to the 0.5 wt.% Nd and 1.0 wt.% Nd additions.

The detailed analysis of the intermetallic is shown in Fig. 5 with TEM bright-field images and the corresponding selected area electron diffraction (SAED) patterns of the Mg1.6La1Ce-3.0Nd alloy in the as-cast state. As seen in Fig. 5(c), the eutectic

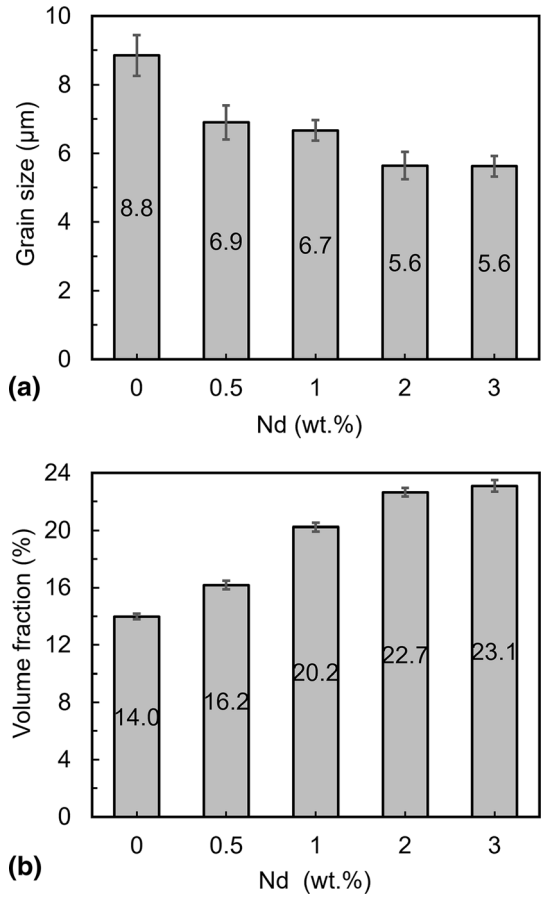

Fig. 3 The volume fraction of eutectic phase and average grain size in the as-cast die-cast Mg1.6La1Ce-*x*Nd alloys

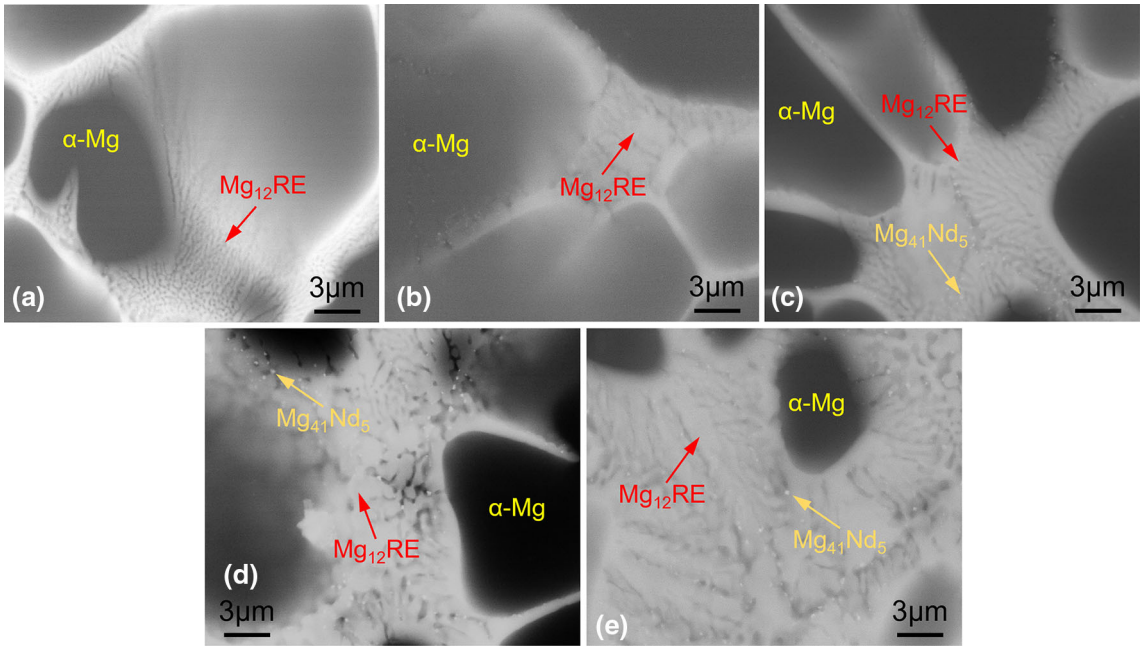

Fig. 4 BSE-SEM microstructure of the as-cast die-cast Mg1.6La1Ce-*x*Nd alloys; (a) x = 0 Nd, (b) x = 0.5, (c) x = 1, (d) x = 2, (e) x = 3

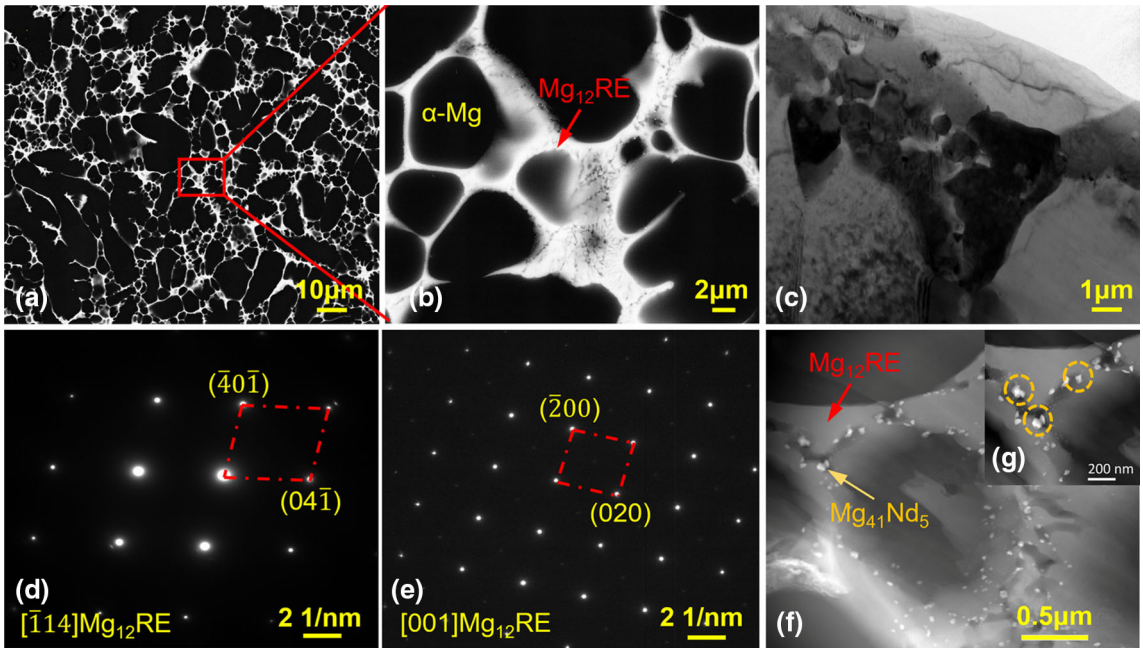

Fig. 5 Microstructure of the die-cast Mg1.6La1Ce-3Nd alloy under as-cast condition; (a) Low magnification BSE-SEM for overall microstructure; (b) High magnification BSE-SEM for detailed eutectic microstructure; (c) BF-TEM image of eutectic phase at GBs; (d, e) SADP of $Mg_{12}RE$ phase observed along [$\bar{1}$ 14] and [001] zone axes; (f, g) High magnification STEM-HAADF image of the eutectic phase at GBs

phase was consistent with that observed in the SEM. Analysis of the SAED diagram showed that the eutectic phase should be $Mg_{12}RE$ (body-centred tetragonal), which was consistent with the results of the XRD analysis. Furthermore, the EDX result for points C and D in Fig. 6(a) and Table 2 showed that the Mg: (La, Ce, Nd) was close to 12, indicating that the phase was $Mg_{12}RE$, and also showed that the concentration of La and Nd was close each other, and Ce content was much lower. Although there was 0.3 wt.% Zn added to the alloy, no reported segregation of Zn in Mg12RE was found based on the EDX and SAED results (Ref 35). In addition, Fig. 5(f) and (g) showed another diffuse distribution of bulk phases on the grain boundaries, with an average size of about 30-50 nm. The TEM-EDX results in Fig. 6(a)-(g) showed that the massive phases were enriched in Nd elements and could be judged as the Mg-Nd phases. The results showed that the Mg: RE ratio was close to 8, so the Mg-RE bulk phase should be $Mg_{41}RE_5$, a stable phase in binary Mg-Nd alloys, which was generally considered less likely to form at HPDC with high cooling rates(Ref 36). The lack of detection of acceptable bulk

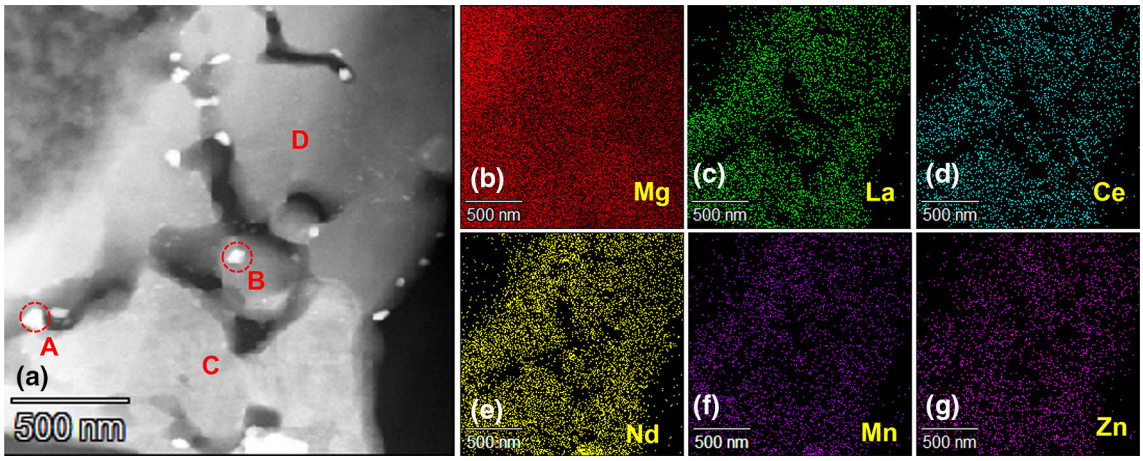

Fig. 6 Microstructure morphology and STEM-EDX results of the as-cast die-cast Mg1.6La1Ce-3Nd alloys. (a) High magnification STEM image of the $Mg_{12}RE$ network and eutectic phase at GB; (b)-(g) STEM-EDX mapping of elements (b) Mg, (c) La, (d) Ce, (e) Nd, (f) Mn, (g) Zn in the eutectic phases at GB

Table 2 EDX analysis (at. %) in the as-cast HPDC Mg1.6La1Ce-3Nd alloy

Point	Mg	Nd	La	Ce	Mn
A	85.8±1.2	13.3±0.5	0.2±0.0	0.3±0.2	0.3±0.3
B	87.5±1.3	11.8±0.6	0.3±0.3	0.4±0.4	0.0±0.0
C	91.7±1.2	3.3±0.3	3.2±0.5	1.6±0.3	0.2±0.2
D	91.3±1.4	3.4±0.6	3.7±0.3	1.3±0.4	0.3±0.3

The selected points are shown in Fig. 6(a).

Mg41Nd5 phase in Fig. 1 should be due to the volume fraction of the Mg41Nd5 phase being too minor to detect.

3.3 Mechanical Properties at Ambient and Elevated Temperatures

Figure 7(a)-(c) shows the variation in mechanical properties of the die-cast Mg1.6La1Ce-*x*Nd alloy at ambient temperature and high temperatures of 250 and 300 °C. With the addition of Nd, the yield strength of the alloy gradually increased at ambient temperature, while the corresponding elongation (El) gradually decreased. Compared with the alloy without Nd, the addition of 3.0 wt.% Nd led to an increase in yield strength of 19.4%. Furthermore, at high temperatures, the yield strength of the alloy also increased gradually with the addition of Nd. At 250 °C, the 3.0 wt.% Nd addition increased the yield strength by 26.1% compared to the Nd-free alloy, while at 300 °C, the yield strength increased to a degree of 62.3%. Thus, it is shown that the addition of Nd could effectively enhance the high-temperature mechanical properties of the alloy. Moreover, the El of the alloy containing Nd elements was enhanced in comparison to that without Nd addition. However, as shown in Fig. 7(c), the trend of decreasing the elongation at high temperatures was still retained with the increase of Nd addition. It indicates that the network eutectic structure in the alloy remained well-stabilised at high temperatures. Detailed data and standard deviations of the average tensile properties of the HPDC cast Mg1.6La1Ce-*x*Nd alloy are presented in Table 3.

Figure 8 shows the features of the fractured surface in the die-cast Mg1.6La1Ce-*x*Nd alloys at ambient temperature. The fractured surfaces were featured by cleavages, indicating that brittle fractures were mainly responsible for the broken. Also, cracks were seen along the grain boundaries, but most of the cracks were close to the fractured surface, supporting evidence of brittle fractures. However, the situation was changed for the fractures at elevated temperatures. As shown in Fig. 9, the fractured surface contained many dimples, which indicates that ductile fractures were mainly responsible for the breakage.

4. Discussion

4.1 Microstructural Evolution

The solidification process can well understand the microstructural evolution. From the equilibrium phase diagram of Mg-Nd binary alloys (Ref 37), the eutectic reaction occurs during solidification at the Mg-7.4 at.% Nd (Mg-32.4wt.%Nd). Therefore, the experimental alloys in this study should be within hypo eutectic alloys.

As shown in Fig. 10 for the phase diagram on the cross-section of Mg1.6La1Ce, the different Nd contents at a level up to 3.3 wt.%, the phases formed during solidification were α-Mg and $Mg_{12}RE$. However, the diagram in Fig. 10 also showed the slight change in liquidus temperature and solidus temperature in the alloys with different Nd contents. The ternary eutectic reaction at 590 °C produced α-Mg, $Mg_{12}RE$ and $Mg_{41}RE_5$. Therefore, according to the phase diagram, the possible phases presented in the alloy with Nd were α-Mg, $Mg_{12}RE$ and $Mg_{41}RE_5$. Moreover, the phase diagram showed the appearance of the $Mg_{41}Nd_5$ phase at addition of approximately 1.4 wt.% of Nd. It is consistent with the alloy microstructure in Fig. 5 and 6. The clear solidification paths can be seen in Fig. 11 for the experimental alloys. The decrease of liquidus temperatures and the solidification ranges for the alloys with higher Nd contents were seen in association with the reduction of eutectic solidification ranges in the alloys with higher Nd contents. As the solidification range is directly linked with castability, adding Nd in the experimental alloy can increase the castability, resulting in better quality and fewer defects in the castings.

4.2 The relationship Between Microstructures and Mechanical Properties

As shown in Fig. 7 and Table 3, Nd additions significantly improved the strength of as-cast Mg1.6La1Ce-*x*Nd alloys. The strength improvement is always associated with the restriction of dislocation movement (Ref 32, 38). Therefore, it can confirm that grain strengthening, secondary phase strengthening and solid solution strengthening contribute to the alloy strengthening (Ref 39). Thus, the strengthening mechanism in the alloy can be expressed as an equation (Ref 33, 39, 35):

$$\sigma_{\mathrm{Mg1.6La1.0Ce-xNd}} = \sigma_{gb} + \sigma_{ss} + \sigma_{Mg-RE} \quad \text{(Eq 1)}$$

In the HPDC alloy, grain refinement is generally associated with strengthening defined by the Hall-Petch relationship in the equation (Ref 40):

$$\sigma_y = \sigma_0 + Kd^{-1/2} \quad \text{(Eq 2)}$$

where d is grain size, K is the material constant. In general, the grain sizes in HPDC alloys are relatively fine (Ref 41). The formation of the two different grain sizes is because solidification occurs when the melted metal comes into contact with the relatively cold die wall, resulting in a larger grain size before high pressure, in contrast to the fine grain size after high pressure is applied (Ref 42). At the same time, the Nd addition has a slight refinement effect on the grain size of the Mg1.6La1Ce-*x*Nd series alloys and a corresponding increase in the volume fraction of the eutectic phase, as found in the paper. Generally, it is assumed that the smaller the grain size, the greater the number of grain boundaries and thus the more significant the hindrance to dislocation (Ref 32). Therefore, it can be concluded that the addition of Nd provides effective grain boundary strengthening.

The effect of grain boundary reinforcement is also directly influenced by the second-phase (Ref 39). The addition of Nd increases the number of lamellar $Mg_{12}RE$ phases, while nanoscale bulk $Mg_{41}Nd_5$ phases are produced at the grain boundaries. The continuous distribution of the intermetallic compound $Mg_{12}RE$ at the grain boundaries has a strong reinforcing effect on the yield strength (Ref 33, 35). Moreover, the metastable phase $Mg_{12}RE$ and the stable phase $Mg_{41}Nd_5$ have good thermal stability (Ref 43). It would also suggest that adding Nd can effectively enhance the high-temperature tensile properties while improving the room temperature tensile properties. It is indicated that the lamellar structure of $Mg_{12}RE$ is commonly found to occur at higher volume fractions (Ref 34). Therefore, the strength change with the Nd addition is predominantly associated with the grain size, volume fraction and distribution of second-phase particles.

Moreover, the solution strengthening should also be significant in the alloys with Nd contents. The solubility of Nd in Mg is 3.6 wt.% (Ref 44). Compared to the La and Ce, the solid solubility of Nd in the magnesium matrix is slightly higher. However, shown in Fig. 6, the Mg-RE intermetallic compound occupies a considerable amount of the Nd element, and the

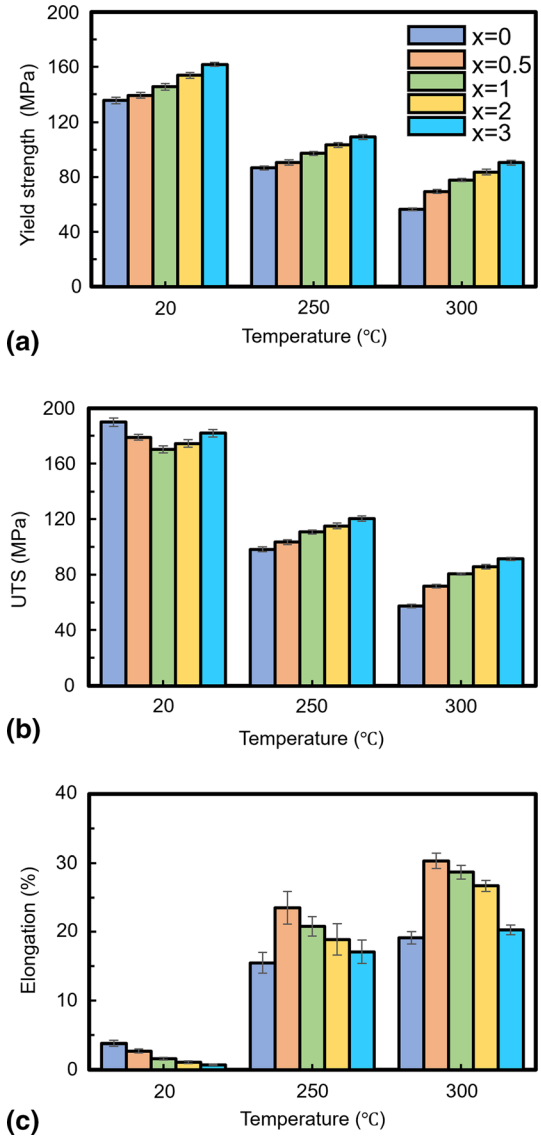

Fig. 7 Mechanical properties of die-cast Mg1.6La1Ce-*x*Nd alloys at ambient temperature (20 °C), 250 and 300 °C. (a) yield strength, (b) ultimate tensile strength, (c) elongation

Table 3 Mechanical properties of die-cast Mg1.6La1Ce-*x*Nd alloys under as-cast condition

	RT			200 °C			300 °C		
Alloy	**UTS, MPa**	**YS, MPa**	**El, %**	**UTS, MPa**	**YS, MPa**	**El, %**	**UTS, MPa**	**YS, MPa**	**El, %**
Mg1.6La1Ce-0Nd	135.6±2.3	189.9±3.0	3.8±0.4	86.6±1.4	98.3±1.8	15.5±1.5	56.3±0.9	57.4±1.3	19.1±0.9
Mg1.6La1Ce-0.5Nd	139.3±2.0	178.9±2.1	2.7±0.3	90.5±2.0	103.5±1.7	23.5±2.4	69.4±1.4	71.7±1.4	30.3±1.1
Mg1.6La1Ce-1Nd	145.5±2.3	170.2±2.4	1.6±0.2	97.2±1.5	110.8±1.5	20.8±1.4	77.8±1.2	80.5±0.8	28.7±1.0
Mg1.6La1Ce-2Nd	153.9±2.1	174.5±2.6	1.1±0.2	103.3±1.7	115.1±2.1	18.9±2.3	83.6±2.1	85.7±1.7	26.7±0.8
Mg1.6La1Ce-3Nd	161.9±1.6	181.9±2.7	0.7±0.1	109.2±1.8	120.6±1.9	17.1±1.7	90.4±1.7	91.4±1.1	20.3±0.7

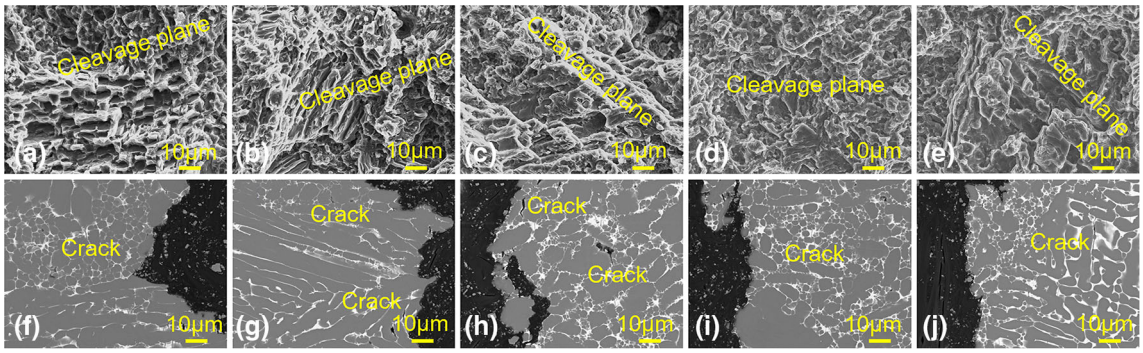

Fig. 8 (a)-(e) SEM micrographs showing the fractured surface and (f)-(j) BSE-SEM micrographs showing the sectioned surface of die-cast Mg1.6La1Ce-*x*Nd alloys at ambient temperature, (a), (f) $x = 0$, (b), (g) $x = 0.5$, (c), (h) $x = 1$, (d), (i) $x = 2$, (e), (j) $x = 3$

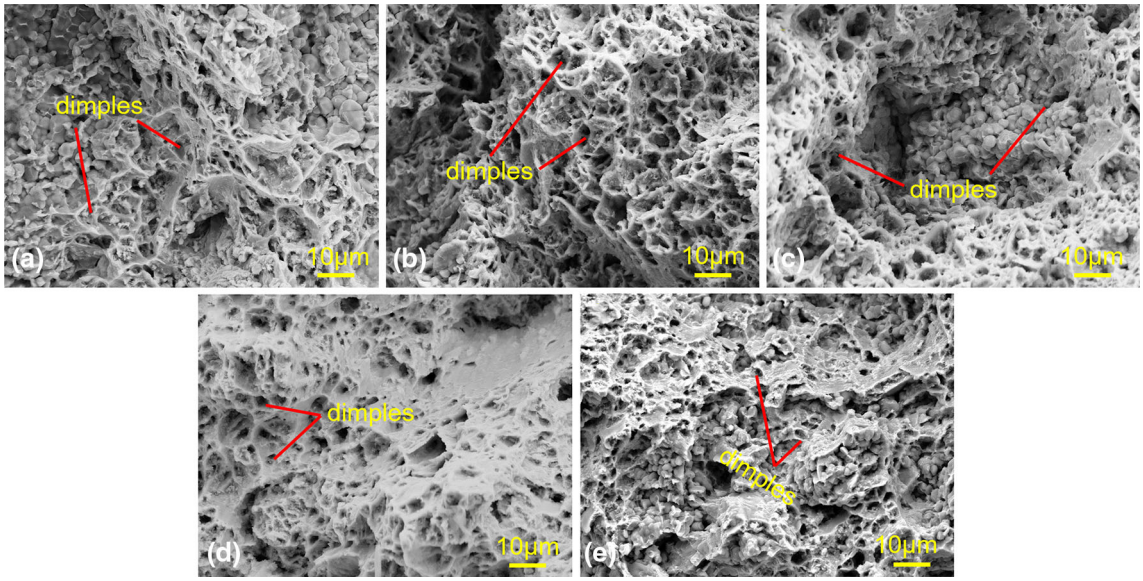

Fig. 9 SEM micrographs showing the fractured surface of die-cast Mg1.6La1Ce-*x*Nd alloys at 300 °C, (a) $x = 0$, (b) $x = 0.5$, (c) $x = 1$, (d) $x = 2$, (e) $x = 3$

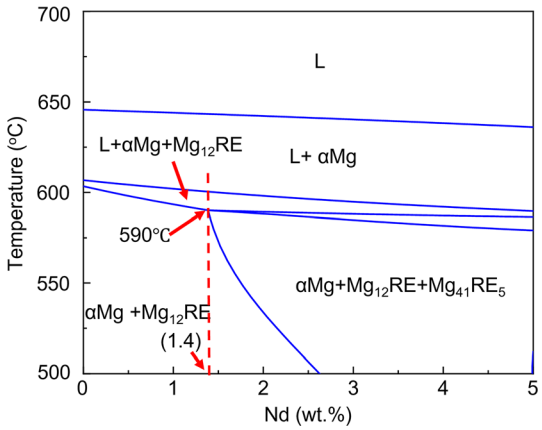

Fig. 10 Phase diagram of Mg1.6La1Ce-*x*Nd alloys on the cross-section of Mg1.6La1Ce with different Nd contents

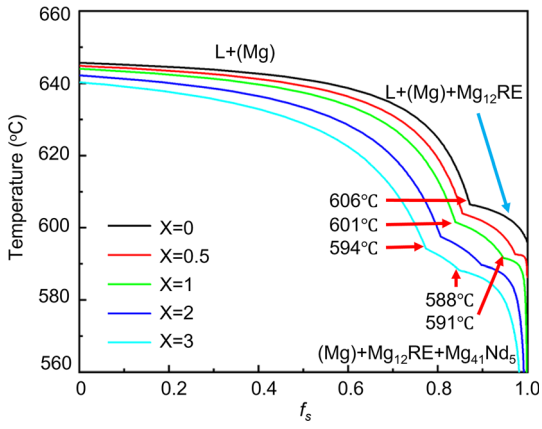

Fig. 11 Solidification path of Mg1.6La1Ce-*x*Nd alloys on the cross-section of Mg1.6La1Ce with different Nd contents

remaining Nd solute atoms are mainly concentrated around the grain boundaries. Therefore, although the solid solution of Nd elements is relatively high, the solid solution strengthening effect produced at low additions is still limited. Overall, the enhancement of yield strength caused by Nd addition is primarily associated with the decrease in grain size and the increase of volume fraction of fine second-phases.

5. Conclusions

In the present study, the effect of Nd on the microstructures and tensile properties of Mg1.6La1Ce-*x*Nd alloys at ambient and elevated temperatures was investigated, and the main conclusions are as follows:

(1) The refined primary α-Mg phase can be achieved in the high-pressure die-cast Mg1.6La1Ce-*x*Nd alloys with different Nd contents. Nd addition leads to the formation of more $Mg_{12}RE$ phases. The mean grain size of the eutectic phase decreases, and the volume fraction of the eutectic phase increase with increasing the content of Nd in the alloys.
(2) For the mechanical properties at ambient temperature, the yield strength increases, and the elongation decreases for the Mg1.6La1Ce-*x*Nd alloys with the increase of Nd contents. For the mechanical properties at elevated temperatures, the yield strength decreases, and the elongations increase for the Mg1.6La1Ce-*x*Nd alloys with the increase of temperatures.
(3) The strength improvement is primarily associated with the restriction of dislocation movement. Three sources of dislocation movement obstructing available in the alloys include grain boundaries, the second-phase particles and solute atoms.

Acknowledgment

The financial supports from Innovate UK (project No.12182100) are gratefully acknowledged.

Authors' Contributions

LF – experimental conduction, data analysed and manuscript preparation. XD – conception, experimental design, results analysis and manuscript editing. QC – Phase identification and data analysis. BW – Supervision of experiments and discussion. SJ – fund acquisition and manuscript proof.

Conflict of interest

The authors declare that they have no known competing financial interest or personal relationships that could have appeared to influence the work reported in this paper.

Open Access

References

1. J.-F. Nie, Precipitation and Hardening in Magnesium Alloys, *Metall. Mater. Trans. A.*, 2012, **43**(11), p 3891–3939.
2. D. Liu, D. Yang, X. Li, and S. Hu, Mechanical Properties Corrosion Resistance and Biocompatibilities of Degradable Mg-RE Alloys: A Review, *J. Mater. Res. Technol.*, 2019, **8**(1), p 1538–1549.
3. N. Mo, Q. Tan, M. Bermingham, Y. Huang, H. Dieringa, N. Hort, and M.-X. Zhang, Current Development of Creep-Resistant Magnesium Cast Alloys: A Review, *Mater. Des.*, 2018, **155**, p 422–442.
4. A. Prasad, S. Si, U.R. Ghori, G. Thirunavukkarasu, Y.L. Chiu, I.P. Jones, S.Y. Lee, S.S. Singh, N.N. Gosvami, and J. Jain, Effect of La Addition on Precipitation Hardening in Mg-10Dy Alloy, *Materialia*, 2020, **14**, p 100898.
5. S. Gavras, S.M. Zhu, J.F. Nie, M.A. Gibson, and M.A. Easton, On the Microstructural Factors Affecting Creep Resistance of Die-Cast Mg–La-Rare Earth (Nd, Y or Gd) Alloys, *Mater. Sci. Eng., A*, 2016, **675**, p 65–75.
6. H. Yong, S. Guo, Z. Yuan, Y. Qi, D. Zhao, and Y. Zhang, Phase Transformation, Thermodynamics and Kinetics Property of Mg90Ce5RE5 (RE = La, Ce, Nd) Hydrogen Storage Alloys, *J. Mater. Sci. Technol.*, 2020, **51**, p 84–93.
7. B. Zhang, A.V. Nagasekhar, X. Tao, Y. Ouyang, C.H. Cáceres, and M. Easton, Strengthening by the Percolating Intergranular Eutectic in an HPDC Mg-Ce Alloy, *Mater. Sci. Eng.: A*, 2014, **599**, p 204–211.
8. M. Celikin, A.A. Kaya, R. Gauvin, and M. Pekguleryuz, Effects of Manganese on the Microstructure and Dynamic Precipitation in Creep-Resistant Cast Mg-Ce-Mn Alloys, *Scripta Mater.*, 2012, **66**(10), p 737–740.
9. X.-P. Cui, H.-F. Liu, J. Meng, and D.-P. Zhang, Microstructure and Mechanical Properties of Die-Cast AZ91D Magnesium Alloy by Pr Additions, *Trans. Nonferrous Metals Soc/ China*, 2010, **20**, p s435–s438.
10. J.-W. Wang, F. Yang, T.-W. Fan, B.-Y. Tang, L.-M. Peng, and W.-J. Ding, Theoretical Investigation of New Type of Ternary Magnesium Alloys AMgNi4 (A=Y, La, Ce, Pr and Nd), *Phys. B*, 2011, **406**(6–7), p 1330–1335.
11. X. Dong, L. He, X. Huang, and P. Li, Effect of Electromagnetic Transport Process on the Improvement of Hydrogen Porosity Defect in A380 Aluminum Alloy, *Int. J. Hydrogen Energy*, 2015, **40**(30), p 9287–9297.
12. N. Dong, J. Wang, H. Ma, and P. Jin, Effects of Nd Content on Thermal Expansion Behavior of Mg-Nd Alloys, *Mater. Today Commun.*, 2021, **29**, p 102894.
13. B. Lei, B. Jiang, H. Yang, Z. Dong, Q. Wang, M. Yuan, G. Huang, J. Song, D. Zhang, and F. Pan, Effect of Nd Addition on the Microstructure and Mechanical Properties of Extruded Mg-Gd-Zr Alloy, *Mater. Sci. Eng.: A*, 2021, **816**, p 141320.
14. X. Li, C. Liu, J. Wang, and C. Zhang, Tailoring the Strength and Formability of Mg Alloys through Rare Earth Element Additions (Gd and Dy) and Dynamic Recrystallizations, *Mater. Today Commun.*, 2021, **28**, p 102627.
15. J. Zhao, B. Jiang, Y. Yuan, Q. Wang, M. Yuan, A. Tang, G. Huang, D. Zhang, and F. Pan, Understanding the Enhanced Ductility of Mg-Gd with Ca and Zn Microalloying by Slip Trace Analysis, *J. Mater. Sci. Technol.*, 2021, **95**, p 20–28.
16. J. Zhang, W. Li, and Z. Guo, Static Recrystallization and Grain Growth during Annealing of an Extruded Mg-Zn-Zr-Er Magnesium Alloy, *Journal of Magnesium and Alloys*, 2013, **1**(1), p 31–38.
17. B. Chen and J. Zhang, Microstructure and Mechanical Properties of ZK60-Er Magnesium Alloys, *Mater. Sci. Eng., A*, 2015, **633**, p 154–160.
18. X. Dong, L. He, X. Huang, and P. Li, Coupling Analysis of the Electromagnetic Transport of Liquid Aluminum Alloy during Casting, *J. Mater. Process. Technol.*, 2015, **222**, p 197–205.
19. L. Li, Y. Wang, C. Zhang, T. Wang, and H. Lv, Effects of Yb Concentration on Recrystallization, Texture and Tensile Properties of Extruded ZK60 Magnesium Alloys, *Mater. Sci. Eng.: A*, 2020, **788**, p 139609.

20. K. Guan, B. Li, Q. Yang, D. Zhang, X. Zhang, J. Zhang, L. Zhao, X. Liu, and J. Meng, Microstructural Characterization of Intermetallic Phases in a Solution-Treated Mg-5.0Sm-0.6Zn-0.5Zr (wt.%) Alloy, *Mater. Charact.*, 2018, **145**, p 329–336.
21. X. Xia, W. Sun, A.A. Luo, and D.S. Stone, Precipitation Evolution and Hardening in Mg Sm Zn Zr Alloys, *Acta Mater.*, 2016, **111**, p 335–347.
22. K. Luo, L. Zhang, G. Wu, W. Liu, and W. Ding, Effect of Y and Gd Content on the Microstructure and Mechanical Properties of Mg-Y-RE Alloys, *J. Mag. Alloys*, 2019, **7**(2), p 345–354.
23. L.-L. Chang, J. Guo, and X.-J. Su, Effect of Y on Microstructure Evolution and Mechanical Properties of Mg-4Li-3Al Alloys, *Trans. Nonferrous Metals Soc. China*, 2021, **31**(12), p 3691–3702.
24. H. Zengin, and Y. Turen, Effect of Y Addition on Microstructure and Corrosion Behavior of Extruded Mg-Zn-Nd-Zr Alloy, *J. Mag. Alloys*, 2020, **8**(3), p 640–653.
25. F. von Buch, J. Lietzau, B.L. Mordike, A. Pisch, and R. Schmid-Fetzer, Development of Mg-Sc-Mn Alloys, *Mater. Sci. Eng., A*, 1999, **263**(1), p 1–7.
26. P. Wang, E. Guo, X. Wang, H. Kang, Z. Chen, Z. Cao, and T. Wang, The Influence of Sc Addition on Microstructure and Tensile Mechanical Properties of Mg-4.5Sn-5Zn Alloys, *J. Mag. Alloys*, 2019, **7**(3), p 456–465.
27. R. Arrabal, B. Mingo, A. Pardo, E. Matykina, M. Mohedano, M.C. Merino, A. Rivas, and A. Maroto, Role of Alloyed Nd in the Microstructure and Atmospheric Corrosion of As-Cast Magnesium Alloy AZ91, *Corros. Sci.*, 2015, **97**, p 38–48.
28. B. Wang, S. Guan, J. Wang, L. Wang, and S. Zhu, Effects of Nd on Microstructures and Properties of Extruded Mg-2Zn-0.46Y-*x*Nd Alloys for Stent Application, *Mater. Sci. Eng.: B*, 2011, **176**(20), p 1673–1678.
29. C. Su, D. Li, T. Ying, L. Zhou, L. Li, and X. Zeng, Effect of Nd Content and Heat Treatment on the Thermal Conductivity of Mg Nd Alloys, *J. Alloy. Compd.*, 2016, **685**, p 114–121.
30. Z.L. Ning, H. Wang, H.H. Liu, F.Y. Cao, S.T. Wang, and J.F. Sun, Effects of Nd on Microstructures and Properties at the Elevated Temperature of a Mg-0.3Zn-0.32Zr Alloy, *Mater. Design*, 2010, **31**(9), p 4438–4444.
31. N. Mo, I. Mccarroll, Q. Tan, A. Ceguerra, J. Cairney, H. Dieringa, Y. Huang, B. Jiang, F. Pan, M. Bermingham, and M.-X. Zhang, Roles of Nd and Mn in a New Creep-Resistant Magnesium Alloy, *Mater. Sci. Eng.: A*, 2020, **779**, p 139152.
32. N. Stanford, J. Geng, Y.B. Chun, C.H.J. Davies, J.F. Nie, and M.R. Barnett, Effect of Plate-Shaped Particle Distributions on the Deformation Behaviour of Magnesium Alloy AZ91 in Tension and Compression, *Acta Mater.*, 2012, **60**(1), p 218–228.
33. S. Gavras, M.A. Easton, M.A. Gibson, S. Zhu, and J.-F. Nie, Microstructure and Property Evaluation of High-Pressure Die-Cast Mg-La-Rare Earth (Nd, Y or Gd) Alloys, *J. Alloy. Compd.*, 2014, **597**, p 21–29.
34. T.L. Chia, M.A. Easton, S.M. Zhu, M.A. Gibson, N. Birbilis, and J.F. Nie, The Effect of Alloy Composition on the Microstructure and Tensile Properties of Binary Mg-Rare Earth Alloys, *Intermetallics*, 2009, **17**(7), p 481–490.
35. J. Rong, J.-N. Zhu, W. Xiao, X. Zhao, and C. Ma, A High Pressure Die Cast Magnesium Alloy with Superior Thermal Conductivity and High Strength, *Intermetallics*, 2021, **139**, p 107350.
36. M.A. Easton, M.A. Gibson, D. Qiu, S.M. Zhu, J. Gröbner, R. Schmid-Fetzer, J.F. Nie, and M.-X. Zhang, The Role of Crystallography and Thermodynamics on Phase Selection in Binary Magnesium-Rare Earth (Ce or Nd) Alloys, *Acta Mater.*, 2012, **60**(11), p 4420–4430.
37. S. Gorsse, C.R. Hutchinson, B. Chevalier, and J.-F. Nie, A Thermodynamic Assessment of the Mg-Nd Binary System Using Random Solution and Associate Models for the Liquid Phase, *J. Alloy. Compd.*, 2005, **392**(1–2), p 253–262.
38. Q. Yang, F. Bu, F. Meng, X. Qiu, D. Zhang, T. Zheng, X. Liu, and J. Meng, The Improved Effects by the Combinative Addition of Lanthanum and Samarium on the Microstructures and the Tensile Properties of High-Pressure Die-Cast Mg-4Al-Based Alloy, *Mater. Sci. Eng., A*, 2015, **628**, p 319–326.
39. Y. Xu, F. Gensch, Z. Ren, K.U. Kainer, and N. Hort, Effects of Gd Solutes on Hardness and Yield Strength of Mg Alloys, *Prog. Nat. Sci.: Mater. Int.*, 2018, **28**(6), p 724–730.
40. R. Zhao, W. Zhu, J. Zhang, L. Zhang, J. Zhang, and C. Xu, Influence of Ni and Bi Microalloying on Microstructure and Mechanical Properties of As-Cast Low RE LPSO-Containing Mg-Zn-Y-Mn Alloy, *Mater. Sci. Eng.: A*, 2020, **788**, p 139594.
41. P.-F. Qin, Q. Yang, Y.-Y. He, J.-H. Zhang, J.-S. Xie, X.-R. Hua, K. Guan, and J. Meng, Microstructure and Mechanical Properties of High-Strength High-Pressure Die-Cast Mg-4Al-3La-1Ca-0.3Mn Alloy, *Rare Metals*, 2021, **40**(10), p 2956–2963.
42. J. Zhang, M. Zhang, J. Meng, R. Wu, and D. Tang, Microstructures and Mechanical Properties of Heat-Resistant High-Pressure Die-Cast Mg-4Al-XLa-0.3Mn (x = 1, 2, 4, 6) Alloys, *Mater. Sci. Eng.: A*, 2010, **527**(10–11), p 2527–2537.
43. C. Zhai, Q. Luo, Q. Cai, R. Guan, and Q. Li, Thermodynamically Analyzing the Formation of Mg12Nd and Mg41Nd5 in Mg-Nd System under a Static Magnetic Field, *J. Alloy. Compd.*, 2019, **773**, p 202–209.
44. Y. Zhang, Y. Huang, F. Feyerabend, C. Blawert, W. Gan, E. Maawad, S. You, S. Gavras, N. Scharnagl, J. Bode, C. Vogt, D. Zander, R. Willumeit-Romer, K.U. Kainer, and N. Hort, Influence of the Amount of Intermetallics on the Degradation of Mg-Nd Alloys under Physiological Conditions, *Acta Biomater.*, 2021, **121**, p 695–712.